Calcif Tissue Int (2016) 99:99–109
DOI 10.1007/s00223-016-0124-8

ORIGINAL RESEARCH

Influence of Fatigue Loading and Bone Turnover on Bone Strength and Pattern of Experimental Fractures of the Tibia in Mice

Nicolas Bonnet[1] · Maude Gerbaix[1] · Michael Ominsky[2] · Patrick Ammann[1] · Paul J. Kostenuik[1] · Serge L. Ferrari[1]

Received: 11 January 2016 / Accepted: 19 February 2016 / Published online: 5 March 2016

Abstract Bone fragility depends on bone mass, structure, and material properties, including damage. The relationship between bone turnover, fatigue damage, and the pattern and location of fractures, however, remains poorly understood. We examined these factors and their integrated effects on fracture strength and patterns in tibia. Adult male mice received RANKL (2 mg/kg/day), OPG-Fc (5 mg/kg 2×/week), or vehicle (Veh) 2 days prior to fatigue loading of one tibia by in vivo axial compression, with treatments continuing up to 28 more days. One day post fatigue, crack density was similarly increased in fatigued tibiae from all treatment groups. After 28 days, the RANKL group exhibited reduced bone mass and increased crack density, resulting in reduced bone strength, while the OPG-Fc group had greater bone mass and bone strength. Injury repair altered the pattern and location of fractures created by ex vivo destructive testing, with fractures occurring more proximally and obliquely relative to non-fatigued tibia. A similar pattern was observed in both non-fatigued and fatigued tibia of RANKL. In contrast, OPG-Fc prevented this fatigue-related shift in fracture pattern by maintaining fractures more distal and transverse. Correlation analysis showed that bone strength was predominantly determined by aBMD with minor contributions from structure and intrinsic strength as measured by nanoindentation and cracks density. In contrast, fracture location was predicted equally by aBMD, crack density and intrinsic modulus. The data suggest that not only bone strength but also the fracture pattern depends on previous damage and the effects of bone turnover on bone mass and structure. These observations may be relevant to further understand the mechanisms contributing to fracture pattern in long bone with different levels of bone remodeling, including atypical femur fracture.

Keywords Fatigue · Bone turnover · Cracks · Fracture pattern

Introduction

Osteoporosis is predominantly a condition related to aging, causing fragility fractures which increase exponentially in the elderly, eventually affecting 50 % of women and 30 % of men past 50 years of age. Bone mineral density is strongly associated with bone strength [1, 2]; however, the bone density of populations who fracture and those who do not fracture overlaps considerably; extra-skeletal factors such as the risk and nature of falls may not be sufficient to explain these discrepancies [3, 4]. Several investigations using HR-pQCT showed that impaired bone microarchitecture was associated with fractures independently of BMD [5, 6]. Despite some methodological limitations, principal component analysis revealed that BMD, microarchitecture, and micro-finite element analyses parameters jointly explained 86.2 % of the total variability of wrist fracture [7, 8]. These observations suggest that material properties known to have a direct influence upon

Electronic supplementary material The online version of this article (doi:10.1007/s00223-016-0124-8) contains supplementary material, which is available to authorized users.

✉ Nicolas Bonnet
nicolas.bonnet@unige.ch

[1] Division of Bone Diseases, Department of Internal Medicine Specialties, Geneva University Hospital & Faculty of Medicine, 64 Av de la Roseraie, 1205 Geneva 14, Switzerland

[2] Metabolic Disorders, Amgen Inc., Thousand Oaks, CA, USA

the initiation and propagation of microcracks could also modestly contribute to fracture risk [9, 10].

It has been proposed that osteoporotic fractures may result from a positive feedback between microdamage and the resulting remodeling that attempts to repair the damage [11], which temporarily reduces bone volume in a manner that can increase cortical porosity [12]. Hence, it has been predicted that excessive loading may cause the system to become unstable, with microdamage increasing and provoking localized remodeling that may further destabilize the damaged site [13]. On the other side, it has been hypothesized that the inhibition of bone remodeling may also cause detrimental changes in bone, such as decreased mineral crystallinity [14] and inhibition of microdamage repair, which could favor bone fragility [15–19]. However, in these studies microdamage and/or material properties were not correlated to overall bone strength, and levels of bone turnover were not directly assessed. These important research questions may have relevance to the etiology of atypical femur fractures (AFFs), which have been described in a small percentage of patients on antiresorptive therapies. Relative to osteoporotic femur fractures, AFFs occur more distally and have a more transverse fracture pattern [20]. The observation of AFF in patients treated with bisphosphonates or denosumab suggests an interaction between microdamage and the level of bone turnover, which could affect not only bone strength but also the pattern and location of fracture [20]. Recent data from a rodent long bone healing model indicated that denosumab shifted the location of fractures produced during ex vivo torsional testing [21]. Hence, the main objective of our study was to clarify determinants of bone strength and fracture patterning in the context of high and low turnover and fatigue damage in an axially loaded mouse tibia model.

Materials and Methods

Animals

Seventy-two 14-week-old male C57BL/6J mice were obtained from Charles River (France), and weight-matched mice were housed 6 per cage in a laboratory animal care facility with a 12-h light/dark cycle. At 16 weeks of age, three treatments were initiated ($n = 24$ per group): vehicle (Veh, saline, sc), osteoprotegerin–immunoglobulin Fc segment complex (OPG-Fc, 5 mg/kg twice per week, sc), and receptor activator of nuclear factor kappa-B ligand (RANKL, 2 mg/kg/day, sc), known to induce 3 levels of bone remodeling—normal, low, and high, respectively. RANKL and OPG-Fc regimens have been chosen to, respectively, increased and decreased bone resorption [22]. Two days after treatment initiation, the left tibia of all mice was subjected to fatigue loading. The non-stimulated tibia served as an internal control. Half the mice from each treatment group were sacrificed 1 day after fatigue loading ($n = 12$ per treatment), and the remaining mice continued their treatments for an additional 28 days before being sacrificed. For the mice sacrificed 30 days after the initiation of the treatment, dynamic indices of bone formation were evaluated by the subcutaneous injections of calcein (25 mg/kg, Sigma, Switzerland) 9 and 2 days before euthanasia. Mice were euthanized by an overdose of ketamine–xylazine. Blood from all mice was obtained from the submandibular vein at baseline and after 3 and 30 days of treatment for analysis of TRACP5b (tartrate-resistant alkaline phosphatase form 5b). Tibiae were excised for micro-computed tomography (microCT) analysis, histomorphometry, microcrack evaluation, destructive axial compression testing, and nanoindentation. Bone mineral density (aBMD, g/cm^2), microarchitecture, indentation, cortical cracks, and histomorphometric measurements were performed as previously described [23–29]. Details of each method are provided in appendix.

All animal procedures were designed in accordance with the Swiss Federal Act on Animal Protection following AALAC/IACUC protocols, approved by the University Of Geneva School Of Medecine Ethical Committee (1055/3781/2).

In Vivo Fatigue Loading

Fatigue loading force intensity was determined based on previous ex vivo axial compression fracture tests [24]. This intensity corresponded to the value obtained when the increase in actuator displacement reached 30 % of the average displacement at complete fracture, as previously defined [30]. The following parameters have been used, inferred from previous study: peak load = 14 N; peak strain (midshaft cortex) = 1500 με; pulse period (trapezoid shaped pulse) = 0.1 s; rest time between pulses = 0.33 s; full cycle frequency (pulse + rest) = 3 Hz [30]. A total of 3240 cycles (∼ 18 min) were applied.

Destructive Biomechanical Testing

Tibia were tested ex vivo in a destructive axial compression test that aligned the strength test in the same direction as the in vivo fatigue stimulus, as previously described [31]. The cartilaginous part of the distal tibia was removed using a saw, and the tibia was oriented with the proximal side up and the distal end fixed in a drill chuck in a consistent manner to ensure that the same percentage of bone

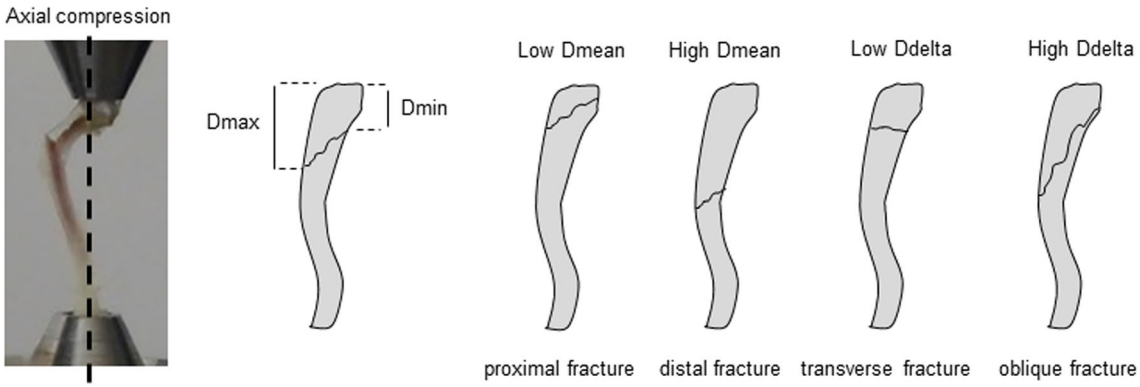

Fig. 1 An example of a completed axial compression test of the whole tibia, and schematic images describing fracture morphology assessments. Dmax and Dmin represent the highest and lowest distances from the proximal tibial plateau to the fracture site, respectively. The mid-way point between Dmax and Dmin, called Dmean, indicates fracture location, with a high Dmean indicating a more distal (diaphyseal) location and a low Dmean indicates a more proximal (metaphyseal) location. Fracture pattern was indicated by the Ddelta, which indicates the relative obliqueness of the fracture line. Fractures with a higher Ddelta are more oblique, while those with a lower Ddelta are more transverse

length is fixed in the chuck (Fig. 1). Tibiae were loaded to fracture to determine whole-bone mechanical properties.

Localization and Pattern of Experimental Fractures

After biomechanical testing, fractured tibias were scanned by microCT as described in the appendix. The maximum (Dmax) and minimum (Dmin) distances from the proximal tibial plateau to the fracture line were measured using Scanco software. Fracture location was assessed by Dmean ([Dmax + Dmin]/2), and fracture pattern by Ddelta (Dmax-Dmin) (Fig. 1).

Statistical Analysis

The effects of fatigue in each treatment group were examined by comparing the loaded and the non-loaded tibia using a paired *t* test. The effects of the two durations of treatment (1 day and 28 days after fatigue) on bone parameters were compared using an unpaired *t* test.

The effects of fatigue and the effects of the remodeling rate and their interactions on bone fracture parameters were investigated using a two-way ANOVA. As appropriate, Fisher's protected Least Squares Difference (PLSD) post hoc tests were performed to assess differences between groups. A Pearson correlation matrix was generated to determine which bone parameters were correlated to tibial strength, with all groups included in the analysis. Differences were considered significant at $p < 0.05$. Data are presented as mean ± SEM. Analyses were performed with Statview and MedCalc Statistical Software version 13.1.2 (MedCalc Software bvba, Belgium).

Results

Effects of RANKL and OPG-Fc on Bone Strength and Fracture Pattern in Non-fatigued Tibia

After 3 days of exposure, OPG-Fc and RANKL, respectively, decreased and increased TRACP-5b, an osteoclast bone turnover marker (Table 1). At this time, no significant treatment-related changes in aBMD were yet observed, nor any differences in cortical microarchitecture, crack density, intrinsic biomechanical properties, bone strength, pattern and location of fracture in non-fatigued bones (Fig. 2a, b; Table 1). After 30 days, the RANKL group exhibited decreased aBMD and microstructure, while cracks number per bone area (CrN/BA) increased, resulting in lower bone strength relative to Veh controls (Table 2). At that time, fractures pattern had become more oblique and proximal in RANKL vs Veh, as shown by a Ddelta of +87.5 %, and Dmean of −39.7 % relative to Veh controls (both $p < 0.05$, Fig. 2c, d). In contrast, OPG-Fc increased bone mass and microarchitecture and decreased CrN/BA (Table 2). As a consequence, bone strength was increased but the pattern and location of fractures remained comparable to the Veh group (Fig. 2c, d; Table 2).

Acute Effects of Fatigue Loading on Bone Strength and Fracture Pattern

One day after fatigue loading, trabecular and cortical microstructure across all regions remained unchanged, regardless of treatment (Fig. 3a, b). Fatigue significantly increased crack density in all treatment groups (Veh, OPG-Fc, and RANKL, Fig. 3c). Nanoindentation-derived intrinsic bone material properties remained unaffected by fatigue,

Table 1 Effect of 3 days of RANKL and OPG-Fc on bone parameters linked to bone strength in non-fatigued bone

	Parameter	Vehicle	OPG-Fc	RANKL
Bone resorption	Serum TRACP5b (U/L)	3.5 ± 0.1	1.8 ± 0.1****,$$$$	5.7 ± 0.1****
Whole tibia	aBMD (mg/cm^2)	52.2 ± 2.7	51.3 ± 0.4	50.3 ± 0.5
1/3 Proximal	aBMD (mg/cm^2)	53.9 ± 0.7	53.7 ± 0.5	50.7 ± 0.6
1/3 Midshaft	aBMD (mg/cm^2)	45.2 ± 0.7	44.3 ± 0.4	44.3 ± 0.6
Proximal	BV/TV (%)	10.4 ± 1.9	11.5 ± 1.7$	7.9 ± 1.5 *
	Tb.N (1/μm)	4.2 ± 0.1	4.5 ± 0.1$$	3.5 ± 0.1**
	Tb.Th (μm)	50 ± 1	49 ± 1	48 ± 1
	Tb.Sp (μm)	236 ± 4	221 ± 5	289 ± 4
Midshaft	Ct.TV (mm)	0.74 ± 0.01	0.73 ± 0.01	0.77 ± 0.02
	Ct.BV (mm)	0.42 ± 0.008	0.41 ± 0.004	0.43 ± 0.01
	CrN/BA (1/mm^2)	72.0 ± 7.3	86.1 ± 8.2	88.3 ± 8.4
	CrS/BS (%)	7.5 ± 1.0	6.6 ± 0.6	6.6 ± 0.4
Proximal	Modulus (gPa)	14.3 ± 0.6	15.5 ± 0.5	16.0 ± 0.8
	Hardness (mPa)	431.8 ± 14.4	390.1 ± 40.3	450.8 ± 36.5
Bone strength	Ult. Force (N)	26.4 ± 0.8	25.0 ± 1.3	24.8 ± 0.6
	Stiffness (N/mm)	35.6 ± 2.7	35.6 ± 2.0	35.2 ± 2.6
	Elastic E (N.mm)	10.3 ± 0.7	10.4 ± 0.8	11.3 ± 0.6

TRACP5b tartrate-resistant alkaline phosphatase form 5b, *aBMD* areal bone mineral density, *BV/TV* bone volume fraction, *Tb.N* trabecular number, *Tb.Th* trabecular thickness, *Tb.Sp* trabecular separation, *Ct.TV* cortical tissue volume, *Ct.BV* cortical bone volume, *CrN/BA* crack number on bone area, *CrS/BS* crack surface on bone surface, *Ult. Force* ultimate force, *Elastic E* elastic energy

Data represent means and SEM; **** $p < 0.0001$ versus Veh, $$$$ $p < 0.0001$ versus RANKL

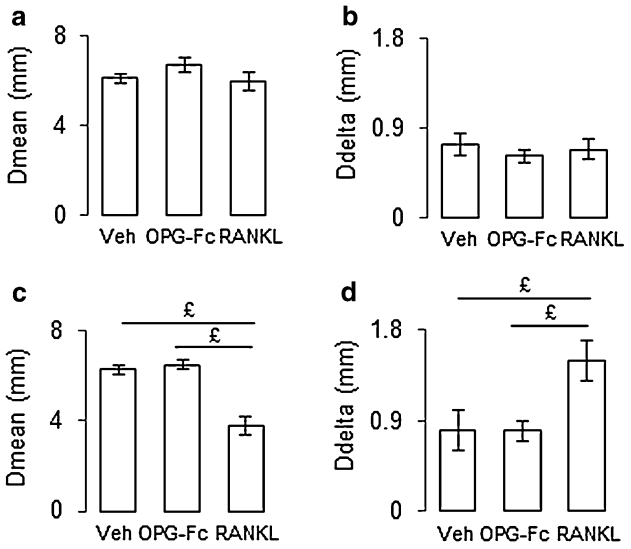

Fig. 2 Effects of RANKL and OPG-Fc treatment in non-fatigued tibia on bone fracture location and pattern. **a**, **b** 1 day after fatigue. **c**, **d** 28 days after fatigue. $^{£}p < 0.05$ between treatment groups

whereas the combination of fatigue and RANKL significantly decreased the modulus compared to fatigued tibiae from the OPG-Fc and Veh groups (Fig. 4). At this early time point, no periosteal reaction/callus was observed at the proximal tibial and bone strength as well as location or pattern of experimental fractures were not changed (Fig. 3d, e).

Influence of Bone Turnover on Injury Response to Fatigue Loading

After 1 month of exposure, OPG-Fc increases, while RANKL decreases BMD at proximal tibia as well as trabecular and cortical structure (Fig. 5a–c), with OPG-Fc effects on BMD being greater in fatigued tibia. Fatigue alone had no influence on trabecular and cortical tibial microstructure, nor nanoindentation parameters (Fig. 4). Periosteal calluses were located from 600 to 1800 μm under the proximal growth plate in fatigued tibia for all groups, and callus BV was more than twice as great in OPG-Fc vs Veh ($p < 0.05$), whereas no significant differences in callus BV were noted between RANKL and Veh (Fig. 5d, e). At that point, crack density in fatigued bones remained significantly higher in the RANKL group (Fig. 5f). In contrast, OPG-Fc reduced crack density in fatigued tibiae such that it became lower than the Veh and RANKL groups and similar to non-fatigued OPG-Fc treated tibia.

In accordance with expected changes in bone remodeling activity, endocortical bone formation rate (BFR/BPm) was very low in the fatigued and non-fatigued OPG-Fc group compared to Veh or RANKL. In contrast, periosteal BFR/BPm was not significantly changed by OPG-Fc both in fatigued and non-fatigued (Fig. 5g–i). Histomorphometry confirmed the absence of intra-cortical remodeling in non-fatigued mice, whereas calcein

Table 2 Effect of 30 days of RANKL and OPG-Fc on bone parameters linked to bone strength in non-fatigued bone

	Parameters	Vehicle	OPG-Fc	RANKL
Bone resorption	Serum TRACP5b (U/L)	3.1 ± 0.1	0.4 ± 0.2****,$$$$	5.1 ± 0.2****
Whole tibia	aBMD (mg/cm^2)	54.5 ± 0.7	58.2 ± 0.8****,$$$$	45.2 ± 0.5****
1/3 Proximal	aBMD (mg/cm^2)	56.1 ± 0.9	62.9 ± 0.9****$$$$	44.9 ± 0.5****
1/3 Midshaft	aBMD (mg/cm^2)	47.6 ± 0.9	49.2 ± 1.1**,$$$$	39.4 ± 0.6
Proximal	BV/TV (%)	12.4 ± 1.1	16.8 ± 0.8***,$$$$	1.5 ± 0.2****
	Tb.N (1/μm)	4.4 ± 0.1	4.8 ± 0.1**,$$$$	1.4 ± 0.1****
	Tb.Th (μm)	52.0 ± 1.1	57.3 ± 1.1**	63.5 ± 2.8**
	Tb.Sp (μm)	222 ± 7	200 ± 5**,$$$$	776 ± 47****
Midshaft	Ct.TV (mm)	0.81 ± 0.02	0.86 ± 0.03	0.81 ± 0.01
	Ct.BV (mm)	0.45 ± 0.01	0.52 ± 0.02*,$$$$	0.36 ± 0.01****
	CrN/BA (1/mm^2)	89.7 ± 2.7	56.4 ± 4.9**,$$$$	169.9 ± 6.6****
	CrS/BS (%)	8.1 ± 0.4	5.3 ± 0.6*,$$$$	13.4 ± 1.2***
Proximal	Modulus (gPa)	14.3 ± 0.8	15.6 ± 0.5	12.9 ± 0.9
	Hardness (mPa)	442.1 ± 23.3	494.5 ± 28.8$	380.5 ± 34.2
Bone strength	Ult. Force (N)	29.6 ± 0.6	33.1 ± 0.9*,$$$	24.3 ± 1.3**
	Stiffness (N/mm)	45.1 ± 2.2	46.0 ± 5.1	35.2 ± 1.6
	Elastic E (N.mm)	11.9 ± 1.0	15.4 ± 2.1$	9.7 ± 1.2

TRACP5b tartrate-resistant alkaline phosphatase form 5b, *aBMD* areal bone mineral density, *BV/TV* bone volume fraction, *Tb.N* trabecular number, *Tb.Th* trabecular thickness, *Tb.Sp* trabecular separation, *Ct.TV* cortical tissue volume, *Ct.BV* cortical bone volume, *CrN/BA* crack number on bone area, *CrS/BS* crack surface on bone surface, *Ult. Force* ultimate force, *Elastic E* elastic energy

Data represent means and SEM; ** $p < 0.01$, *** $p < 0.001$, **** $p < 0.0001$ versus vehicle; $$ $p < 0.01$, $$$ $p < 0.001$, $$$$ $p < 0.0001$ versus RANKL

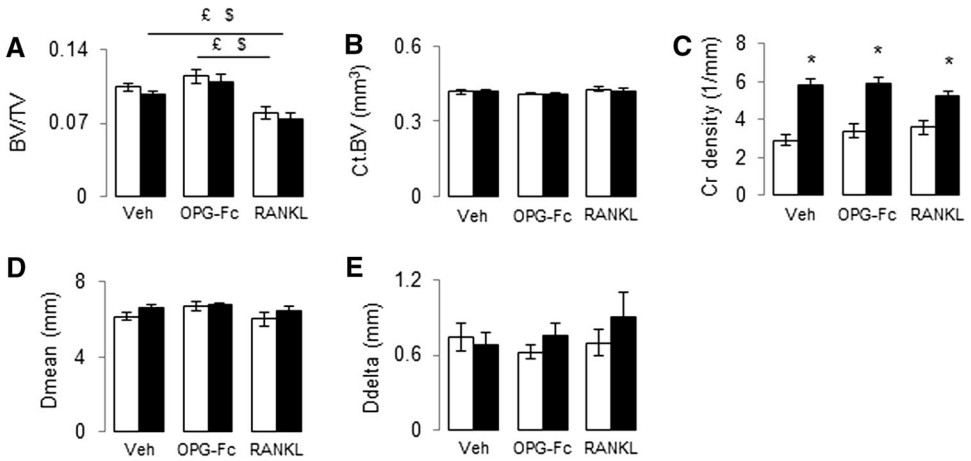

Fig. 3 Effects of RANKL and OPG-Fc treatment on trabecular (**a**) and cortical (**b**) microarchitecture, cracks density (**c**), bone fracture location (**d**), and pattern (**e**) 1 day after fatigue. *$p < 0.05$ versus non-fatigued tibia; $^{\$}p < 0.05$ between treatment groups in fatigued tibia. $^{£}p < 0.05$, between treatment groups in non-fatigued tibia. *White bars* non-fatigued tibia; *black bars* fatigued tibia. Fracture pattern (Ddelta, see Fig. 1 for clarification), bone fracture location (Dmean, see Fig. 1 for clarification), bone volume fraction (BV/TV), cortical bone volume (Ct.BV), cracks density (Cr. Density)

labeling was observed in fatigued tibia (Fig. 5i). OPG-Fc abolishes approximatively all the intra-cortical labeling, whereas RANKL exacerbates it (Fig. 5i). Unfortunately, we were not able to quantify these effects. Whole tibia strength was impacted both by turnover rate and fatigue loading (Fig. 5j–l).

Interaction Between Bone Turnover and Fatigue Loading on Bone Strength and Fracture Pattern

Contrasting with early post-fatigue results (above), after 28 days, fatigued tibiae from the Veh group exhibited testing-induced fractures that were more proximal (Dmean

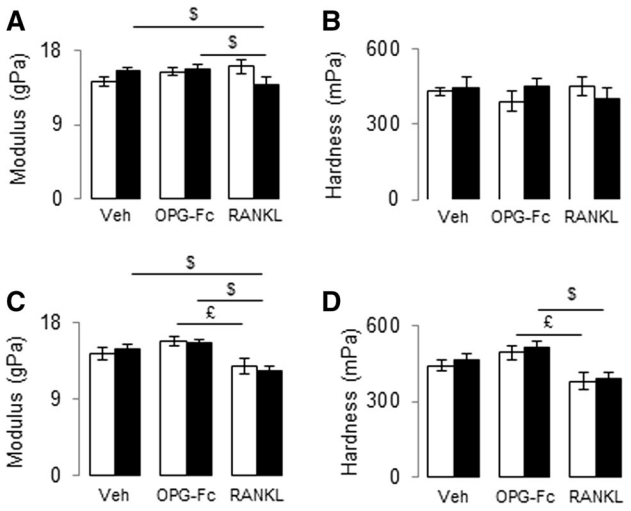

Fig. 4 Effects of RANKL and OPG-Fc treatment on nanoindentation parameters 1 and 28 days after fatigue. **a**, **b** 1 day after fatigue; **c**, **d** 28 days after fatigue. $^{\$}p < 0.05$ between treatment groups in fatigued tibia. *White bars* non-fatigued tibia; *black bars* fatigued tibia. $^{£}p < 0.05$, between treatment groups in non-fatigued tibia

−43 %, $p < 0.05$) and oblique (Ddelta +376 %, $p < 0.05$) compared to non-fatigued Veh control tibiae (Fig. 6a–d). In the OPG-Fc group, Dmean and Ddelta did not differ between fatigued and non-fatigued tibia, with fractures in both states occurring more distally and more transversely vs corresponding samples from Veh controls. Similar to their non-fatigued tibia, fatigued tibia from RANKL animals fractured more proximally (Dmean −31.9 %, $p < 0.05$) compared to the fatigued Veh (Fig. 6a–d).

Hierarchical Determinants of Fracture Morphology and Bone Strength

To determine which measured parameters contributed to whole tibia strength parameters, correlations were performed across all groups and time points. Whole-bone aBMD and microarchitecture parameters were positively associated with ultimate force, stiffness and elastic energy ($p < 0.01$), whereas CrN/BA was negatively associated with all those bone mechanical parameters ($p < 0.001$) (Table 3). Both modulus and hardness were positively correlated with ultimate force ($p < 0.05$).

Linear regression analyses indicated that 22 % of the variance in Dmean could be explained by whole tibia aBMD, 20 % by crack density, and 23 % by intrinsic modulus. Among bone microarchitecture parameters, the shift in fracture location was better correlated with bone volume fraction (BV/TV, $\beta = 0.39$, $p < 0.001$) than with cortical bone volume (CtBV, $\beta = 0.29$, $p < 0.01$) (Table 1). Pattern of the fracture (Ddelta) was significantly and negatively associated with aBMD ($\beta = -0.20$, $p < 0.05$), with higher aBMD predicting a more transverse fracture line.

Discussion

The main objective of our study was to clarify determinants of bone strength and fracture location in the context of RANKL or OPG-Fc treatment and fatigue loading. Three levels of bone remodeling were tested, high (RANKL), low (OPG-Fc), or normal (vehicle) during a very brief and a longer post-fatigue recovery period. As expected, BMD and microarchitecture have strong positive associations with bone strength, while crack density exhibited weaker negative associations. Interestingly, low bone remodeling induced by OPG on the background of fatigue damage was associated with weak but significant changes in the pattern of experimental fractures, which required a greater force to occur but were more transverse and more distally located toward the diaphysis.

As expected, 30 days of OPG-Fc and RANKL treatments increased and decreased bone mass and structure, respectively. Our study indicates that either 3 or 30 days of OPG-Fc pre or post-fatigue did not change the material properties evaluated by nanoindentation. Such data may be relevant due to interest in the effects of OPG-Fc or denosumab treatment on material-level strength parameters, triggered in part by evidence that RANKL inhibitors can cause greater reductions in bone resorption vs bisphosphonates. However, we provide novel evidence that RANKL reduced material properties, specifically elastic modulus, presumably through high remodeling the substantial deposition of new bone tissues did not have enough time to mature, reducing the average tissue hardness, as shown with high injection of PTH [32].

In accordance with other supra-physiological loading models [33–35], neither OPG-Fc nor RANKL impaired the bone modeling-based formation response to fatigue, with callus formation observed in both the low and high state of bone remodeling. Moreover, as reported in bone repair models, we observed a larger callus volume after RANKL inhibition, probably due to the inhibition of the callus remodeling process [21, 36]. This consistent finding, which was also seen with bisphosphonates [19], may have clinical implications for the subset of atypical femur fractures (AFFs) that exhibit periosteal "beaking" a feature thought to represent a callus response to stress fracture [20]. Based on data from complete fracture models [19] and the current fatigue damage model, a periosteal callus in response to stress-related bone damage may become more apparent radiographically as a result of antiresorptive therapy. In the current model, the larger callus in OPG-Fc animals may have conferred improved biomechanical stability.

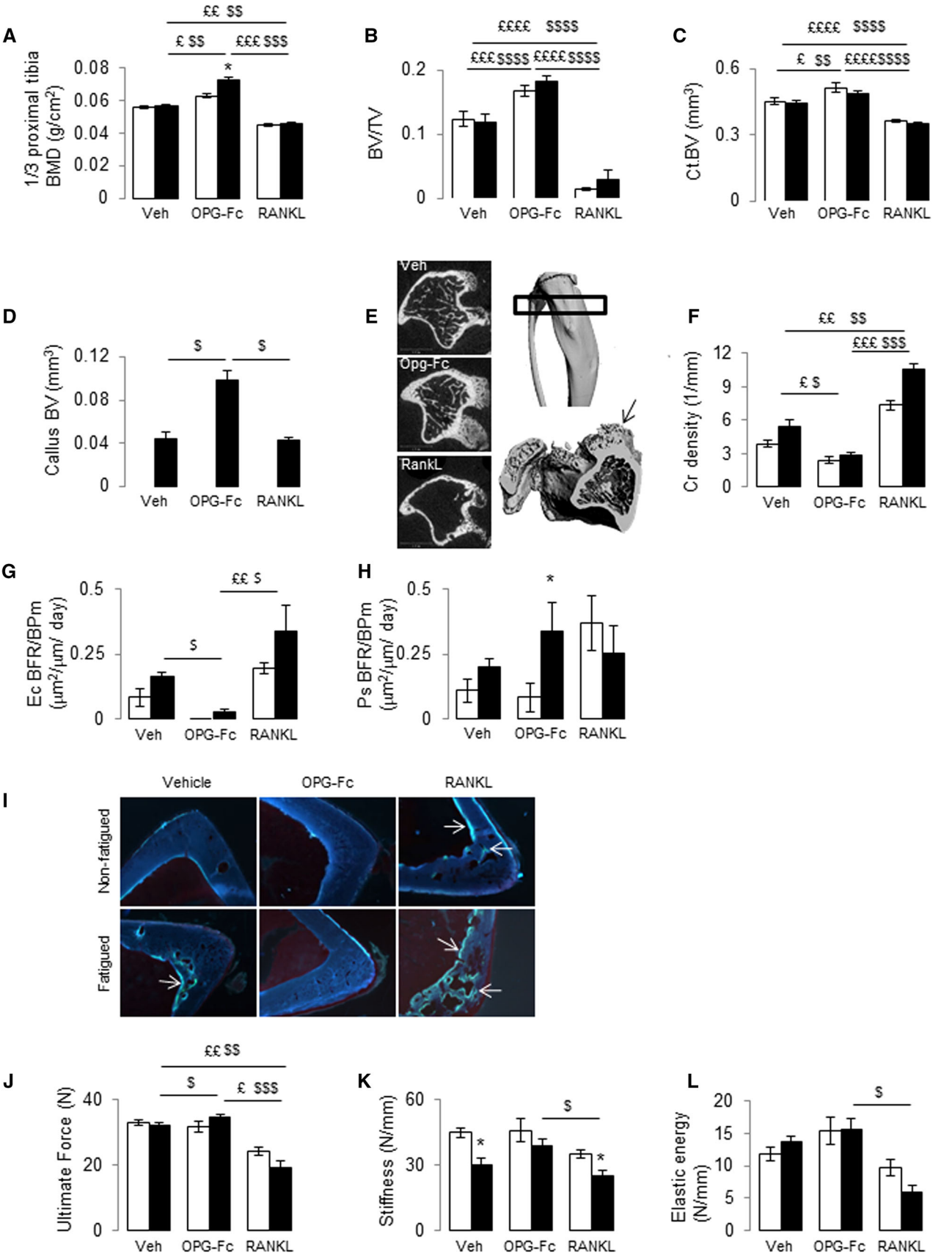
A
1/3 proximal tibia BMD (g/cm²)
0.08
0.06
0.04
0.02
0
£ $$
£$$
£$$$
*
Veh
OPG-Fc
RANKL
B
BV/TV
0.2
0.1
0
£$$$$
£$$$$
£$$$$
Veh
OPG-Fc
RANKL
C
Ct.BV (mm³)
0.6
0.3
0
£ $$
£$$$$
£$$$$
Veh
OPG-Fc
RANKL
D
Callus BV (mm³)
0.12
0.08
0.04
0
$
$
Veh
OPG-Fc
RANKL
E
Veh
Opg-Fc
RankL
F
Cr density (1/mm)
12
9
6
3
0
£$
£$$
£$$$
Veh
OPG-Fc
RANKL
G
Ec BFR/BPm (µm²/µm/ day)
0.5
0.25
0
$
£$
Veh
OPG-Fc
RANKL
H
Ps BFR/BPm (µm²/µm/ day)
0.5
0.25
0
*
Veh
OPG-Fc
RANKL
I
Vehicle
OPG-Fc
RANKL
Non-fatigued
Fatigued
J
Ultimate Force (N)
40
20
0
$
£$
£$$
Veh
OPG-Fc
RANKL
K
Stiffness (N/mm)
60
30
0
*
$
*
Veh
OPG-Fc
RANKL
L
Elastic energy (N/mm)
20
15
10
5
0
$
Veh
OPG-Fc
RANKL

◀**Fig. 5** Effects of RANKL and OPG-Fc treatment in response to fatigue on bone mass, microarchitecture, callus, cracks density, bone formation index and strength 28 days after fatigue. **a** 1/3 proximal bone mineral density of the tibia (BMD), **b** trabecular microstructure, **c** cortical microstructure, **d** callus bone volume (BV), **e** Representative 2D and 3D reconstructions of callus tibia located in the region of interest of the trabecular analysis (i.e., 50 slices under the proximal growth plate) by microCT, **f** cracks density, **g**, **h** bone formation rates at the endocortical and periosteum surfaces, **i** Endo and intra-cortical remodeling indicated by calcein labeling under RANKL and in response to fatigue (*arrow* indicate intense labeling), **j–l**) ultimate force, stiffness, and elastic energy after ex vivo axial compression, *White bars* non-fatigued tibia; *black bars* fatigued tibia. $^{*}p < 0.05$ versus non-fatigued tibia; $^{\$}p < 0.05$, $^{\$\$}p < 0.01$, $^{\$\$\$}p < 0.001$ between treatment groups in fatigued tibia. $^{£}p < 0.05$, $^{££}p < 0.01$, $^{£££}p < 0.001$ between treatment groups in non-fatigued tibia. Bone volume fraction (BV/TV), cortical bone volume (Ct.BV), cracks density (Cr. Density), endocortical (Ec) and periosteal surfaces (Ps), bone formation rates on bone perimeters (BFR/BPm)

Microcracks have been proposed as a possible etiological factor in AFFs [20]. In the current model, fatigue loading created an expected increase in microcracks [30, 37], and osteoclast inhibition by OPG-Fc did not further increase crack density early after fatigue compared to vehicle. Crack density was actually decreased in the OPG-Fc group at 28 days post loading. We hypothesize that reduced cracks with OPG-Fc was due to the increase in bone volume and improved strength and stiffness that may have reduced strain that would otherwise induce further cracks. In contrast, osteoclast activation via 30 days of RANKL was shown to promote structural weakness (decreased ultimate force, stiffness, and energy to fracture), and these changes were associated with increases in crack density in both fatigued and non-fatigued tibia. Correlation analysis showed that bone density/structure/material properties positively impacted strength while cracks had a negative effect, with bone mineral density being the dominant determinant of strength compared to bone structure, material properties, or cracks. In contrast, fracture location was predicted equally by aBMD, crack density and intrinsic modulus, which each predicted approximately 22 % of the variation.

For these studies, destructive axial compression testing was chosen to allow the tibia to yield at its weakest location and in its weakest configuration, which yielded a variety of fracture locations and patterns that clearly differed between Veh, OPG-Fc, and RANKL groups. Moreover, it reveals the specific damage and adaptations resulting from the axially applied fatigue loading stimulus compared to the relative 3 point bending or torsional tests [31, 38]. When the fatigue stimulus was applied after remodeling had been altered but prior to major changes in bone mass and structure (i.e., at Day 1), differences in the location or pattern of fractures between treatment groups were not observed. However, by Day 28, altered remodeling via OPG-Fc or RANKL had significantly impacted bone mass, microstructure, cracks, and material properties, and these changes were accompanied by significant

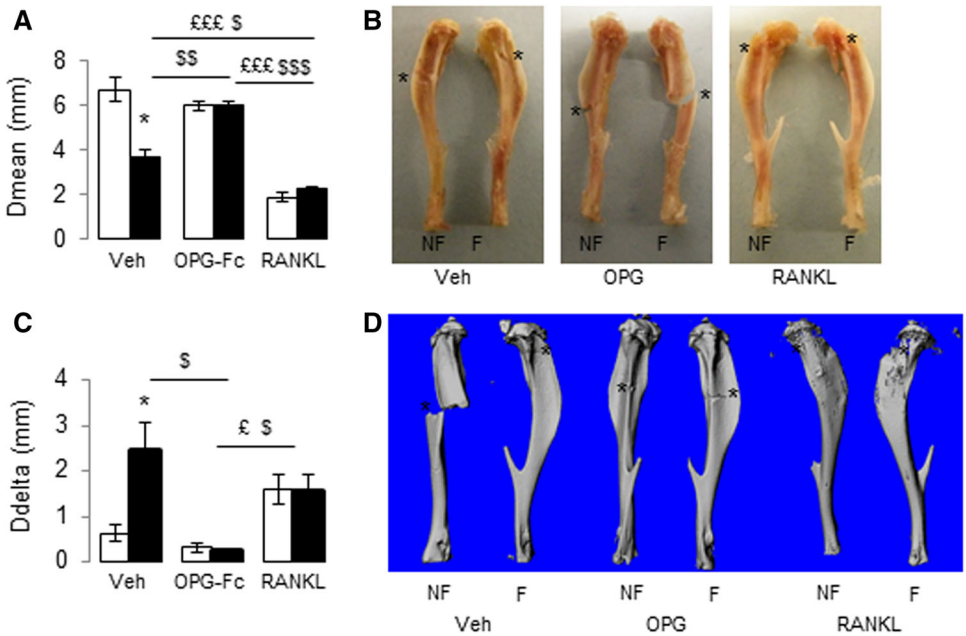

Fig. 6 Effects of RANKL and OPG-Fc treatment in response to fatigue on fracture location and pattern 28 days after fatigue. *White bars* non-fatigued tibia; *black bars* fatigued tibia. **a** bone fracture location (Dmean), **b** Photographs showing the location and pattern of fracture, *asterisks* represent the location of the fraction line; **c** fracture pattern (Ddelta); **d** Representative 3D reconstructions tibia by microCT. $^{\$}p < 0.05$, $^{\$\$}p < 0.01$, $^{\$\$\$}p < 0.001$ between treatment groups in fatigued tibia. $^{£}p < 0.05$, $^{£££}p < 0.001$ between treatment groups in non-fatigued tibia

Table 3 Simple linear correlation between bone strength, fracture pattern/location, and bone quantity/quality determinant

r^2 (β)	Parameter	Ult. force	Stiffness	Elastic E	Dmean	Ddelta	CrN/BA
Whole tibia	aBMD (mg/cm^2)	0.49 (0.67)****	0.07 (0.26)**	0.21 (0.46)****	0.22 (0.46)****	0.04 (−0.20)*	0.33 (−0.57)****
Proximal	BV/TV (%)	0.29 (0.54)****	0.07 (0.26)**	0.10 (0.32)***	0.15 (0.39)***	0.02 (−0.14)	0.26 (−0.51)****
Midshaft	Ct.BV (mm)	0.40 (0.63)****	0.07 (0.26)**	0.16 (0.40)****	0.08 (0.29)**	0 (0.02)	0.15 (−0.39)***
	CrN/BA (1/mm^2)	0.09 (−0.29)**	0.13 (−0.36)**	0.09 (−0.29)**	0.20 (−0.45)***	0.04 (0.19)	X
Nano	Force (mN)	0.09 (0.29)**	0.05 (0.23)*	0.04 (0.19)	0.06 (0.25)*	0 (−0.008)	0.03 (−0.17)
indentation	Modulus (gPa)	0.06 (0.24)*	0.01 (0.07)	0.06 (0.24)*	0.23 (0.48)****	0.02 (−0.14)	0.13 (−0.36)**
	Hardness (mPa)	0.12 (0.34)**	0.06 (0.24)*	0.03 (0.17)	0.06 (0.24)*	0 (0.02)	0.08 (−0.28)

All the groups were including in the analysis 1 and 28 days after fatigue. β is the coefficient of the regression between parameters

aBMD areal bone mineral density, *BV/TV* bone volume fraction, *Ct.BV* cortical bone volume, *CrN/BA* crack number on bone area, *Ult. Force* ultimate force, *Elastic E* elastic energy, fracture pattern (Ddelta, see Fig. 1 for clarification), bone fracture location (Dmean, see Fig. 1 for clarification)

Significance of the correlation * $p < 0.05$, ** $p < 0.01$, *** $p < 0.001$, **** $p < 0.0001$

differences in both the morphology and location of experimental fractures. After OPG-Fc treatment, fractures produced by axial testing exhibited a more diaphyseal location and a more transverse pattern. This morphology of long bone fracture has been described with low-trauma AFFs in patients on antiresorptive therapies, including bisphosphonates and denosumab. Interestingly, other case reports of atypical fracture in bisphosphonate-treated patients have been described at the tibia, another important weight-bearing bone [39–41]. In contrast, there have been no case reports of atypical fracture at the forearm, a non-fatigued, non-weight-bearing site. These findings argue for an important role of the interaction between fatigue and low bone remodeling to shift pattern and localization of the fracture. An overall theory to account for the current fracture morphology findings is that OPG-Fc strengthened while RANKL weakened inherently vulnerable tibial sites, which governed the ultimate location and pattern of experimental fractures. In support of this theory, RANKL promoted a fracture morphology in non-fatigued bones that was reminiscent of that associated with fatigue damage in Veh controls. Conversely, greater callus volume in the fatigued bones from OPG-Fc groups may have fortified this region of focal damage to the point that it became stronger than undamaged distal sites, leading the latter to fail during testing, similar to previous bone healing findings with denosumab [42].

While this study has certain features that may be relevant to AFF pathophysiology, there are also some design features that may limit the model's generalizability and clinical relevance. Central among these is that while AFFs typically occur with minimal or no trauma [20], the experimental fractures examined in the current study were created by overwhelming ex vivo biomechanical forces and were thus traumatic rather than fragility fractures. Factors leading to AFFs are poorly understood, and may include stress fractures and/or crack propagation prior to complete structural failure. In that regard, a possible limitation of the current model is the robustness of callus formation in these young mice, which made complete healing somewhat inevitable, which may contrast with the AFF scenario seen in geriatric patients. In conclusion, the current data indicate that RANKL inhibitors can increase overall structural strength of a fatigue-damaged bone while inducing a shift in fracture features toward more diaphyseal and transverse patterns.

Acknowledgments We thank Ms Madeleine Lachize and Juliette Cicchini for her technical assistance. Authors's roles are as follows: Study design: NB and SF. Study conduct: NB. Data analysis: NB, MG. Data interpretation: NB, PA, PK, MO and SF. Drafting manuscript: NB and SF. Revising manuscript content and approving final version: NB, MG, PA, PK, MO, and SF.

Funding This work was further supported by a grant from Amgen (to NB and SF) and by the SNF Grants No 310030-130550 (to SF).

Compliance with Ethical Standards

Conflict of interest Nicolas Bonnet, Maude Gerbaix, Michael Ominsky, Patrick Ammann, Paul J. Kostenuik and Serge L. Ferrari declare that they have no conflict of interest.

Ethical approval All applicable international, national, and/or institutional guidelines for the care and use of animals were followed. All procedures performed in studies involving animals were in accordance with the ethical standards of the institution or practice at which the studies were conducted.

References

1. Stone KL, Seeley DG, Lui LY, Cauley JA, Ensrud K, Browner WS et al (2003) BMD at multiple sites and risk of fracture of multiple types: long-term results from the Study of Osteoporotic Fractures. J Bone Miner Res 18(11):1947–1954
2. Kanis JA (2002) Diagnosis of osteoporosis and assessment of fracture risk. Lancet 359(9321):1929–1936
3. Austin M, Yang YC, Vittinghoff E, Adami S, Boonen S, Bauer DC et al (2012) Relationship between bone mineral density

changes with denosumab treatment and risk reduction for vertebral and nonvertebral fractures. J Bone Miner Res 27(3):687–693
4. Grisso JA, Kelsey JL, Strom BL, Chiu GY, Maislin G, O'Brien LA, The Northeast Hip Fracture Study Group et al (1991) Risk factors for falls as a cause of hip fracture in women. N Engl J Med 324(19):1326–1331
5. Boutroy S, Bouxsein ML, Munoz F, Delmas PD (2005) In vivo assessment of trabecular bone microarchitecture by high-resolution peripheral quantitative computed tomography. J Clin Endocrinol Metab 90(12):6508–6515
6. Nagy H, Sornay-Rendu E, Boutroy S, Vilayphiou N, Szulc P, Chapurlat R (2013) Impaired trabecular and cortical microarchitecture in daughters of women with osteoporotic fracture: the MODAM study. Osteoporos Int 24:1881–1889
7. Pistoia W, van Rietbergen B, Lochmüller EM, Lill CA, Eckstein F, Rüegsegger P (2002) Estimation of distal radius failure load with micro-finite element analysis models based on three-dimensional peripheral quantitative computed tomography images. Bone 30(6):842–848
8. Boutroy S, Van Rietbergen B, Sornay-Rendu E, Munoz F, Bouxsein ML, Delmas PD (2008) Finite element analysis based on in vivo HR-pQCT images of the distal radius is associated with wrist fracture in postmenopausal women. J Bone Miner Res 23(3):392–399
9. Donahue SW, Galley SA (2006) Microdamage in bone: implications for fracture, repair, remodeling, and adaptation. Crit Rev Biomed Eng 34(3):215–271
10. Lambers FM, Bouman AR, Rimnac CM, Hernandez CJ (2013) Microdamage caused by fatigue loading in human cancellous bone: relationship to reductions in bone biomechanical performance. PLoS One 8(12):e83662
11. McCreadie BR, Goldstein SA (2000) Biomechanics of fracture: is bone mineral density sufficient to assess risk? J Bone Miner Res 15(12):2305–2308
12. Zebaze RM, Ghasem-Zadeh A, Bohte A, Iuliano-Burns S, Mirams M, Price RI et al (2010) Intracortical remodelling and porosity in the distal radius and post-mortem femurs of women: a cross-sectional study. Lancet 375(9727):1729–1736
13. Martin B (1995) Mathematical model for repair of fatigue damage and stress fracture in osteonal bone. J Orthop Res 13(3):309–316
14. Bala Y, Depalle B, Farlay D, Douillard T, Meille S, Follet H et al (2012) Bone micromechanical properties are compromised during long-term alendronate therapy independently of mineralization. J Bone Miner Res 27(4):825–834
15. Burr DB, Forwood MR, Fyhrie DP, Martin RB, Schaffler MB, Turner CH (1997) Bone microdamage and skeletal fragility in osteoporotic and stress fractures. J Bone Miner Res 12(1): 6–15
16. Mashiba T, Hirano T, Turner CH, Forwood MR, Johnston CC, Burr DB (2000) Suppressed bone turnover by bisphosphonates increases microdamage accumulation and reduces some biomechanical properties in dog rib. J Bone Miner Res 15(4):613–620
17. Allen MR, Burr DB (2008) Skeletal microdamage: less about biomechanics and more about remodeling. Clin Rev Bone Miner Metab 6:24–30
18. O'Neal JM, Diab T, Allen MR, Vidakovic B, Burr DB, Guldberg RE (2010) One year of alendronate treatment lowers microstructural stresses associated with trabecular microdamage initiation. Bone 47(2):241–247
19. Bajaj D, Geissler JR, Allen MR, Burr DB, Fritton JC (2014) The resistance of cortical bone tissue to failure under cyclic loading is reduced with alendronate. Bone 64:57–64
20. Shane E, Burr D, Abrahamsen B, Adler RA, Brown TD, Cheung AM et al (2014) Atypical subtrochanteric and diaphyseal femoral fractures: second report of a task force of the American Society for Bone and Mineral Research. J Bone Miner Res 29(1):1–23
21. Gerstenfeld LC, Sacks DJ, Pelis M, Mason ZD, Graves DT, Barrero M et al (2009) Comparison of the effects of the bisphosphonate alendronate versus the RANKL inhibitor denosumab on murine fracture healing. J Bone Miner Res 24:196–208
22. Ominsky MS, Li X, Asuncion FJ, Barrero M, Warmington KS, Dwyer D et al (2008) RANKL inhibition with osteoprotegerin increases bone strength by improving cortical and trabecular bone architecture in ovariectomized rats. J Bone Miner Res 23(5):672–682
23. Iida-Klein A, Lu SS, Yokoyama K, Dempster DW, Nieves JW, Lindsay R (2003) Precision, accuracy, and reproducibility of dual X-ray absorptiometry measurements in mice in vivo. J Clin Densitom 6(1):25–33
24. Bonnet N, Standley KN, Bianchi EN, Stadelmann V, Foti M, Conway SJ et al (2009) The matricellular protein periostin is required for sclerostin inhibition and the anabolic response to mechanical loading and physical activity. J Biol Chem 284(51):35939–35950
25. Bouxsein ML, Boyd SK, Christiansen BA, Guldberg RE, Jepsen KJ, Müller R (2010) Guidelines for assessment of bone microstructure in rodents using micro-computed tomography. J Bone Miner Res 25(7):1468–1486
26. Parfitt AM, Drezner MK, Glorieux FH, Kanis JA, Malluche H, Meunier PJ et al (1987) Bone histomorphometry: standardization of nomenclature, symbols, and units. Report of the ASBMR Histomorphometry Nomenclature Committee. J Bone Miner Res 2(6):595–610
27. Brennan-Speranza TC, Rizzoli R, Kream BE, Rosen C, Ammann P (2011) Selective osteoblast overexpression of IGF-I in mice prevents low protein-induced deterioration of bone strength and material level properties. Bone 49(5):1073–1079
28. Burr DB, Hooser M (1995) Alterations to the en bloc basic fuchsin staining protocol for the demonstration of microdamage produced in vivo. Bone 17(4):431–433
29. Waldorff EI, Christenson KB, Cooney LA, Goldstein SA (2010) Microdamage repair and remodeling requires mechanical loading. J Bone Miner Res 25(4):734–745
30. Bonnet N, Gineyts E, Ammann P, Conway SJ, Garnero P, Ferrari S (2013) Periostin deficiency increases bone damage and impairs injury response to fatigue loading in adult mice. PLoS One 8(10):e78347
31. Warden SJ, Hurst JA, Sanders MS, Turner CH, Burr DB, Li J (2005) Bone adaptation to a mechanical loading program significantly increases skeletal fatigue resistance. J Bone Miner Res 20(5):809–816
32. Brennan T, Rizzoli R, Ammann P (2009) Selective modification of bone quality by PTH, pamidronate or raloxifene. J Bone Miner Res 24:800–808
33. Barrett JG, Sample SJ, McCarthy J, Kalscheur VL, Muir P, Prokuski L (2007) Effect of short-term treatment with alendronate on ulnar bone adaptation to cyclic fatigue loading in rats. J Orthop Res 25:1070–1077
34. Pead MJ, Skerry TM, Lanyon LE (1988) Direct transformation from quiescence to bone formation in the adult periosteum following a single brief period of bone loading. J Bone Miner Res 3:647–656
35. Uthgenannt BA, Kramer MH, Hwu JA, Wopenka B, Silva MJ (2007) Skeletal self-repair: stress fracture healing by rapid formation and densification of woven bone. J Bone Miner Res 22:1548–1556
36. Ross AB, Bateman TA, Kostenuik PJ, Ferguson VL, Lacey DL, Dunstan CR et al (2001) The effects of osteoprotegerin on the mechanical properties of rat bone. J Mater Sci Mater Med 12(7):583–588

37. Nakayama H, Takakuda K, Matsumoto HN, Miyata A, Baba O, Tabata MJ et al (2010) Effects of altered bone remodeling and retention of cement lines on bone quality in osteopetrotic aged c-Src-deficient mice. Calcif Tissue Int 86(2):172–183
38. Turner CH, Burr DB (1993) Basic biomechanical measurements of bone: a tutorial. Bone 14(4):595–608
39. Bissonnette L, April PM, Dumais R, Boire G, Roux S (2013) Atypical fracture of the tibial diaphysis associated with bisphosphonate therapy: a case report. Bone 56(2):406–409
40. Imbuldeniya AM, Jiwa N, Murphy JP (2012) Bilateral atypical insufficiency fractures of the proximal tibia and a unilateral distal femoral fracture associated with long-term intravenous bisphosphonate therapy: a case report. J Med Case Rep. 6(1):50
41. Breglia MD, Carter JD (2010) Atypical insufficiency fracture of the tibia associated with long-term bisphosphonate therapy. J Clin Rheumatol 16(2):76–78
42. Ominsky MS, Stouch B, Schroeder J, Pyrah I, Stolina M, Smith SY et al (2011) Denosumab, a fully human RANKL antibody, reduced bone turnover markers and increased trabecular and cortical bone mass, density, and strength in ovariectomized cynomolgus monkeys. Bone 49(2):162–173